

Article

Effect of Structural Parameters on Output Characteristics of a Novel Self-Supplied Aviation Intelligent Pump

Xudong Han ¹, Yongling Fu ¹, Yan Wang ², Feixiang Yan ² and Liming Yu ^{3,*}

¹ School of Mechanical Engineering and Automation, Beihang University, Beijing 100191, China; xdhan@buaa.edu.cn (X.H.)

² School of Transportation Science and Engineering, Beihang University, Beijing 100191, China

³ School of Automation Science and Electrical Engineering, Beihang University, Beijing 100191, China

* Correspondence: yuliming@buaa.edu.cn

Abstract: The aviation intelligent pump system is an effective solution to aircraft hydraulic systems' inefficient power consumption and temperature increase. A self-supplied aviation intelligent pump (SAIP) has a high power-to-weight ratio and compact structure, making it the optimal choice for an intelligent pump. To analyze the output characteristics of a novel aviation intelligent pump, it is crucial to establish an accurate mathematical model that describes its dynamic characteristics. This can be achieved by analyzing the working principle and exploring the influence of critical parameters. The paper introduces the composition and working principle of a self-supplied electro-hydraulic servo variable displacement pump. It then establishes a mathematical model of the whole pump, with a detailed analysis and modeling of the critical variable mechanism and the swash plate assembly's load moment. A simulation model was created to examine the impact of crucial structural parameters, such as the offset spring's stiffness and control piston's diameter, on the output characteristics of the intelligent pump. An experimental platform was also constructed, and the experimental results confirm the accuracy of the SAIP model presented in this paper. The investigation of the output characteristics fully reveals the dynamic performance of the SAIP. This provides the basis for the subsequent design of high-performance flow and pressure control strategies and aids in researching intelligent aircraft hydraulic systems.

Keywords: self-supplied aviation intelligent pump (SAIP); output characteristics; structural parameters; swash plate's loading torque



Citation: Han, X.; Fu, Y.; Wang, Y.; Yan, F.; Yu, L. Effect of Structural Parameters on Output Characteristics of a Novel Self-Supplied Aviation Intelligent Pump. *Actuators* **2024**, *13*, 186. <https://doi.org/10.3390/act13050186>

Academic Editors: Antonio Carlo Bertolino and Andrea De Martin

Received: 2 April 2024
Revised: 9 May 2024
Accepted: 9 May 2024
Published: 13 May 2024



Copyright: © 2024 by the authors. Licensee MDPI, Basel, Switzerland. This article is an open access article distributed under the terms and conditions of the Creative Commons Attribution (CC BY) license (<https://creativecommons.org/licenses/by/4.0/>).

1. Introduction

The current airborne hydraulic power system is evolving towards high pressure and power to meet the development requirements of a large capacity and high efficiency of civil aircrafts [1]. This trend increases the ineffective power of the system, resulting in a sharp rise in the system's temperature, which leads to the accelerated aging of the medium, difficult sealing of the system, and other problems that will seriously affect the safety of flight control. Therefore, an intelligent aviation hydraulic system that can realize timely matching with the load effectively solves this problem [2]. As the core component of the airborne hydraulic power system, the current airborne pump is mainly the constant-pressure variable displacement pump, and its rated pressure is the maximum pressure during flight, which causes much power to be wasted in other flight phases. Therefore, the intelligent pump system, which can work in different modes according to the flight conditions, effectively solves aircraft hydraulic systems' inefficient power consumption and temperature rise [3].

The intelligent pump is a pump source system that uses a microcontroller to intelligently adjust the output flow rate and pressure of the hydraulic pump. In order to realize the timely perception of the system status, it is necessary to install the pressure, flow rate,

temperature, and other sensors on the pump. The controller applies intelligent algorithms to adjust the displacement or rotation speed of the pump according to the pressure and flow rate instructions generated by the flight control processor, and finally realizes the best matching of the pump's output performance with the load to achieve the goal of saving energy [3]. When the actuators of the flight control system are subjected to a constant load, a constant output force needs to be generated, and the intelligent pump can work in a constant-pressure mode. When the actuators need to output constant speed to drive the rudder surface, a stable flow rate is required, and the intelligent pump can work in a constant-flow mode. When the working conditions of the actuators are complex and changeable, the output force and speed need to change continuously with the needs of the load and rudder surface movement, and the intelligent pump can work in the mode of pressure and flow change. The type selection and structural design of aviation hydraulic pumps need to match the needs of aviation hydraulic systems. Because the working pressure of a rotodynamic pump is low, the flow rate and pressure affect each other, and its working performance is greatly affected by the viscosity of the liquid; it is not suitable for aviation hydraulic systems, so almost all the research on aviation hydraulic pumps use positive displacement pumps. In the category of positive displacement pumps, compared with a gear pump and vane pump, a swash plate pump is widely used in aviation hydraulic systems because of its compact structure, high working pressure, high power-to-weight ratio, and ease of achieving continuously variable displacements. Scholars have designed a variety of working principles and structural forms to meet the needs of intelligent pumps [4–8]. In these schemes, the electro-hydraulic intelligent pump uses the auxiliary pump as the oil source of the servo valve, which can achieve a stable oil source pressure. Still, the additional pump source will increase the volume and weight while making the structure complex and reducing the reliability of the aviation pump.

The self-supplied electric hydraulic intelligent aviation pump scheme avoids these problems well. Based on the current widely used aviation constant-pressure variable displacement pump, the scheme only needs to replace the spool of the compensation valve and integrate the servo valve into the pump shell, which is connected to the control piston chamber and then directly drives the swash plate to adjust the displacement. The main difference with the existing aviation smart pump is that this scheme's oil source for the servo valve comes from the pump outlet, rather than a separate auxiliary pump for oil supply. In contrast, this solution avoids the additional volume and weight of the auxiliary oil source. It is compact in structure and easy to implement based on a constant-pressure variable displacement pump. It still maintains a high power-to-weight ratio and reliability.

To investigate the output performance of variable displacement piston pumps, it is necessary to establish a mathematical model based on the analysis of the principles of its key components to investigate the influence of parameters on the performance. Wu et al. established a theoretical model of the piston cavity that includes fluid compression properties and leakages to reduce the outlet flow pulsation of the high-pressure piston pumps. They proposed a parametric design that optimizes the valve plate's transition region structure to minimize the outlet flow ripple [9]. Fang et al. proposed an improved variable displacement piston pump model to investigate the influence of the variable displacement mechanism on swash plate oscillation. They suggested some feasible methods to reduce swash plate vibration by investigating the role of structural parameters, such as the volume of the outlet chamber and the offset distance of the actuating piston on swash plate vibration [10]. Pan et al. established a theoretical model for the outlet flow pulsation of a constant-power variable displacement piston pump, which considers the vibration of the swash plate, flow leakage, and valve dynamic characteristics. The theoretical model of flow pulsation was used to study the effect of swash plate vibration on the flow and pressure pulsation at the pump outlet. Valve plate optimization based on the theoretical model was also studied by taking the amplitude of the instantaneous outlet flow ripple as the optimization objective function [11]. Chen et al. investigated the causes of the pressure drop of the aeronautical hydraulic systems in the cruise state by setting up a simulation

model of a double-tier constant-pressure controlled variable displacement piston pump. They also studied the effects of the variable pump's piston number, spring stiffness, and pressure drop. The effects of parameters such as the number of pistons, spring stiffness, and the spool's mass on the pressure drop were also investigated [12]. Kumar et al. explored the effects of hydraulic mineral oil on the output power, piston chamber pressure, and leakage flow in the piston cylinder at different temperatures through the established nonlinear mathematical model of axial piston pumps [13]. Ishita et al. analyzed the components of swash plate swiveling torque using a fixed displacement pump's mathematical model, determined the torque values at maximum and minimum flow conditions, and designed the compensator cylinders. The effect of eccentricity on the performances of the fixed and variable displacement pumps was also investigated by simulation [14].

The above research mainly focuses on the performance and critical structural parameters of constant-pressure variable displacement piston pumps. However, in contrast, the self-supplied smart pump can not only actively regulate the pump outlet pressure by the servo valve, but also, importantly, the servo valve's oil source comes from the pump outlet and does not need to add an auxiliary pump source. This makes the output characteristics of the self-supplied smart pump very different from those of constant-pressure variable displacement pumps and other servo pumps. Kemmetmuller et al. designed a pressure control strategy for the self-supplied variable displacement axial piston pumps used in injection molding machines. They developed a load estimator combined with feed-forward and feedback strategies, achieving high-dynamic-pressure tracking under an unknown load [15]. Mu et al., for the pressure control task of self-supplied variable axial piston pumps, using the smooth hinge function provided a control strategy consisting of feedforward and feedback control, compared to switching feedforward control, which can avoid the issues that occur when switching [16]. Guo et al. designed a control scheme combining the output redefined switching control scheme, and the experimental results illustrate the effectiveness of the control strategy [17]. Huang et al. developed a mathematical model of a self-supplied variable displacement pump, including a control system. They used a filter-X least mean squares algorithm with time-delay compensation to compute active control signals and reduce pressure pulsation [18].

In summary, the current research on self-supplied variable displacement pumps primarily focuses on high-precision pressure control and reducing pressure pulsation through active control. However, few studies have investigated the impact of critical structural parameters on performance or the output characteristics of these pumps. Conducting these studies will not only provide a better understanding of the output characteristics of self-supplied variable displacement pumps; it will also guide the design of their key components. Based on the above considerations, this paper describes the principal scheme of a novel self-supplied aviation intelligent pump, establishes its nonlinear mathematical model, and analyzes in detail the effects of crucial structural parameters, such as the offset spring's stiffness and control piston's diameter on the output characteristics of the self-supplied pump, and experimentally explores the output performance of the pump under different conditions.

The paper is structured as follows: firstly, a detailed description of the SAIP's working principle is provided, along with the nonlinear modeling process based on it; secondly, a simulation study is conducted on the output characteristics, based on a mathematical model, considering the offset spring's stiffness, control piston's diameter, and other critical structural parameters; subsequently, the accuracy of the established system model is verified through experiments, and the SAIP's output performance is investigated under different operating conditions; and lastly, the paper concludes.

2. SAIP System Description

2.1. System Principle

Figure 1 shows the SAIP's working principle. Its primary function is to regulate pressure and flow by adjusting the displacement, achieved by changing the swash plate

inclination. To regulate pressure, for example, the servo valve spool assumes the role of the torque motor to the left when the pump outlet pressure is lower than the set value. Then, the control piston chamber is connected to the return oil circuit, and the swash plate inclination increases continuously under the action of the offset spring's torque and other swash plate moments to make the displacement larger until the system pressure rises to the set value. When the pump outlet pressure exceeds the set pressure, the servo valve spool moves to the right, connecting the control piston chamber to the high-pressure oil circuit. This causes the control piston to continuously decrease the swash plate inclination under hydraulic pressure, reducing the pump displacement until the system pressure reaches the set value. Due to the servo valve's high-frequency response, the control piston's short moving distance, and the swash plate assembly's small inertia force, the response speed of displacement changes is faster.

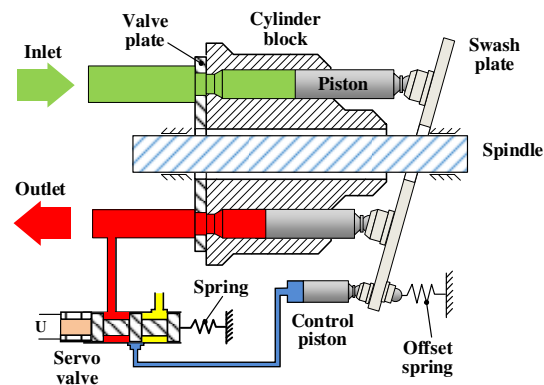


Figure 1. Schematic diagram of the SAIP.

The SAIP comprises three main parts: the piston pump, the variable displacement mechanism, and the electro-hydraulic servo valve. The piston pump is responsible for the output of high-pressure hydraulic oil. The variable displacement mechanism adjusts the swash plate inclination to change the displacement, while the servo valve controls the variable displacement mechanism's motion to achieve precise flow and pressure control. The SAIP is a complex and nonlinear time-varying dynamics system. It has the nonlinearity of flow and pressure inherent in the pump outlet and servo valve and nonlinearity in the valve's dead zone and moving parts friction. Additionally, it is affected by the time-varying nature of the elastic modulus of the oil, the damping coefficient of the moving parts, and the valve flow coefficient. Furthermore, the system's load and environmental conditions can be easily altered, leading to significant interference and a broad range of changes in system parameters.

2.2. Electro-Hydraulic Servo Valve Model

The electro-hydraulic servo valve is the critical component of the SAIP, controlling the flow into and out of the control piston chamber, thereby controlling the extension and retraction of the control piston rod. When the spool travel is positive, high-pressure oil flows through the servo valve into the control piston chamber; when the spool travel is negative, the control piston chamber returns oil through the servo valve to the tank. The flow–pressure equation of the servo valve is:

$$Q_c = C_d w x_v \sqrt{\frac{2}{\rho} (P_p - P_L)} (x_v \geq 0) \quad (1)$$

$$Q_c = C_d w x_v \sqrt{\frac{2}{\rho} (P_L - P_0)} (x_v < 0) \quad (2)$$

where Q_c is the flow in and out of the control piston chamber through the servo valve, called the servo valve control flow, m^3/s ; C_d is the valve's flow coefficient (according to the theory of fluid mechanics, because the flow here is not completely contracted according to the structural parameters of the valve, so the flow coefficient $C_d = 0.7\sim 0.8$ is directly selected in this paper, and it has almost nothing to do with the Reynolds number); w is the valve's opening area gradient, m ; x_v is the spool displacement, m ; ρ is the density of hydraulic oil, kg/m^3 ; P_p is the pump outlet oil pressure, Pa ; P_L is the control piston chamber's oil pressure, Pa ; and P_0 is the oil tank's pressure, Pa .

The dynamic characteristics of an electro-hydraulic servo valve (with a servo amplifier) can be represented by a second-order differential equation:

$$\frac{1}{w_{sv}^2} \ddot{x}_v + \frac{2\zeta_{sv}}{w_{sv}} \dot{x}_v + x_v = k_u u \tag{3}$$

where w_{sv} is the undamped natural frequency of the servo valve, $1/s$; ζ_{sv} is the damping ratio of the servo valve; k_u is the servo valve gain, m/V ; and u is the input voltage, V .

Because usually the frequency response of the servo valve is much faster than the system frequency response, the servo valve dynamics can be regarded as a proportional element:

$$x_v = k_u u \tag{4}$$

According to Equations (1), (2) and (4), then

$$Q_c = k_c u \left[S(u) \sqrt{P_p - P_L} + S(-u) \sqrt{P_L - P_0} \right] \tag{5}$$

where $k_c = k_q k_u$ is the total flow gain of the servo valve, $k_q = C_d w \sqrt{2/\rho}$; and $S(u)$ is an approximate sign function defined as $S(u) = \begin{cases} 1 & u > 0 \\ 0 & u \leq 0 \end{cases}$.

2.3. Model of the Variable Displacement Mechanism-Swash Plate Assembly

The flow continuity equation is satisfied in the control piston chamber when the control flow, Q_c , enters and exits the control piston chamber:

$$Q_c = A_p \dot{x}_p + \frac{V}{\beta_e} \dot{P}_L + C_L P_L \tag{6}$$

where A_p is the effective area of the control piston, m^2 , $A_p = \pi d_p^2 / 4$, d_p is the diameter of the control piston, m ; x_p is the displacement of the control piston, m (this paper stipulates that the direction of the swash plate inclination decreases for the positive direction of displacement); V is the effective volume of the control piston chamber, m^3 ; $V = V_0 + A_p x_p$, V_0 is the initial volume; β_e is the volume elasticity modulus of the hydraulic oil, Pa ; and C_L is the leakage coefficient of the control piston chamber, $m^3/(Pa \cdot s)$.

When the control flow, Q_c , enters and exits the control piston chamber, the control piston rod will extend or retract, and its kinetic analysis is shown in Figure 2, which mainly takes into account the reaction force, F , from the swash plate; the hydraulic pressure, F_L , formed by the oil in the piston chamber; and the viscous resistance, F_B , in the process of movement.

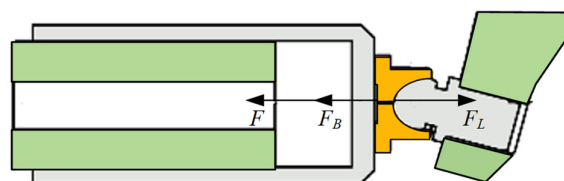


Figure 2. Force analysis of control piston rod.

The force balance equation is:

$$m_p \ddot{x}_p = F_L - F - F_B = P_L A_p - F - B_p \dot{x}_p \quad (7)$$

where m_p is the mass of the control piston, kg; B_p is the viscous damping coefficient of the control piston, N·s/m; and F is the reaction force of the swash plate on the piston rod, N.

The control piston rod pushes the swash plate to rotate, so that its inclination changes to adjust the pump displacement. The swash plate's kinetic analysis is shown in Figure 3. This paper focuses on the dynamic change in swash plate inclination, so only the moment around the swash plate rotary axis, Ox , is analyzed. This paper stipulates that the moment that the swash plate inclination increases is positive. The torque that rotates the swash plate around the axis Ox includes the control torque, M_c , formed by the driving force F of the control piston, the offset torque M_k formed by the offset spring force F_k , the swash plate's own inertial torque M_s , and the combined torque of the other forces on the swash plate, M . The control torque, M_c , of the control piston and the offset torque, M_k , of the offset spring are called the load torque of the variable displacement mechanism.

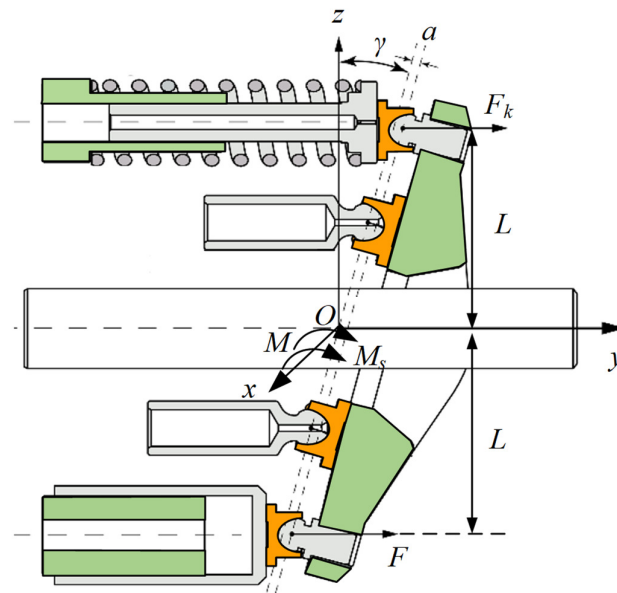


Figure 3. Force analysis of the swash plate.

The moment balance equation for the swash plate around the Ox axis is as follows:

$$\begin{cases} M_c = M_k + M_s + M \\ M_c = FL \\ M_k = F_k L = K(x_p + x_0)L \\ M_s = -I_s \ddot{\gamma} \end{cases} \quad (8)$$

where L is the vertical distance from the control piston and offset spring force to the swash plate rotary axis, m; I_s is the rotational inertia of the swash plate assembly around the swash plate rotary axis, $\text{kg}\cdot\text{m}^2$; γ is the swash plate inclination, rad; K is the stiffness of the offset spring, N/m; and x_0 is the pre-compression of the offset spring, m.

Equations (7) and (8) can be linked to obtain the control piston–swash plate integrated dynamic equations:

$$P_L A_p + \frac{I_s}{L} \ddot{\gamma} - K(x_p + x_0) - \frac{M}{L} - B_p \dot{x}_p = m_p \ddot{x}_p \quad (9)$$

As the swash plate and control piston are mechanically connected, a natural geometrical relationship exists between the swash plate inclination, γ , and the control piston displacement, x_p , as shown in Figure 4.

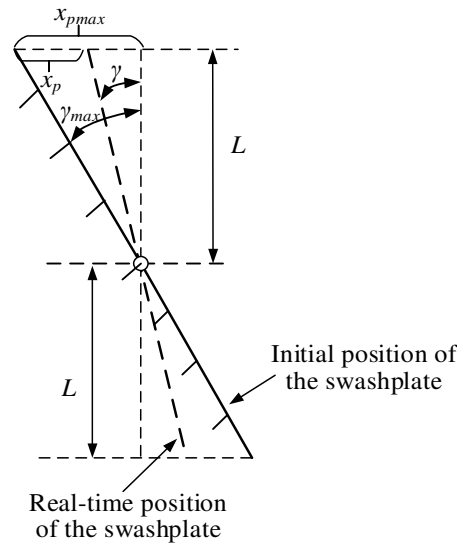


Figure 4. The geometric relationship between the swash plate inclination and control piston’s displacement.

The geometric relationship can be derived from Figure 4:

$$\begin{cases} \tan \gamma = \frac{x_{pmax} - x_p}{L} \\ \tan \gamma_{max} = \frac{x_{pmax}}{L} \end{cases} \quad (10)$$

Since the swash plate always moves within a slight angle, it can be approximated that $\tan \gamma \approx \gamma$, then there is:

$$\begin{cases} x_p = L(\gamma_{max} - \gamma) \\ \dot{x}_p = -L\dot{\gamma} \\ \ddot{x}_p = -L\ddot{\gamma} \end{cases} \quad (11)$$

By substituting Equation (11) into Equations (6) and (9) and collating them, we obtain:

$$\dot{P}_L = \frac{\beta_e}{V} Q_c + \frac{A_p L \beta_e}{V} \dot{\gamma} - \frac{C_L \beta_e}{V} P_L \quad (12)$$

$$\ddot{\gamma} = -\frac{A_p}{mL} P_L + \frac{K}{m} \left(\frac{x_0}{L} + \gamma_{max} \right) - \frac{K}{m} \gamma + \frac{M}{mL^2} - \frac{B_p}{m} \dot{\gamma} \quad (13)$$

where $m = m_p + I_s/L^2$ is the combined mass of the control piston and swash plate assembly, kg.

In addition, the modulus of elasticity of the pump’s solid material is much larger than that of fluid. Therefore, the model in this paper considers the solids in contact with the oil to be rigid, so the vibrations and associated effects are not considered.

2.4. Detailed Analysis of Swash Plate Torque

When the rotational speed is constant, the flow and pressure control of the servo pump are achieved by changing the swash plate inclination to adjust the displacement. Therefore, it is necessary to conduct a detailed study of several key moments on the swash plate, as the various moments on the swash plate directly affect its dynamic response, which in turn affects the flow and pressure regulation. As stated previously, the swash plate is rotated around the Ox axis by the load moment of the regulating mechanism, the moment of the swash plate inertia, and the combined moment of other forces on the swash plate, M .

The load moment of the regulating mechanism and the moment of the swash plate inertia have already been calculated in the previous section. This section will provide a detailed analysis of the combined moment of other forces on the swash plate, M . The combined moment comprises the hydraulic moment M_p , which is formed on the swash plate by the oil pressure in each plunger chamber, the moment of inertia M_1 , which is formed on the swash plate during the movement of each plunger, the friction moment M_2 , which the swash plate experiences when it rotates, the friction moment M_3 between the plunger ball and the ball groove of the sliding shoe, and the self-weight moment M_4 generated by the swash plate's own weight.

2.4.1. Hydraulic Torque of the Plunger Chamber on the Swash Plate

As the cylinder block rotates, the plunger chamber switches between the pump's low-pressure inlet and high-pressure outlet connection, causing the oil pressure to alternate between high and low. An alternating hydraulic moment is created on the swash plate at a frequency equal to the piston pump's pressure pulsation frequency. Due to the high rotational speed and the high discharge pressure of the pump, hydraulic torque has a significant value and high-frequency change, which has an essential influence on the dynamic characteristics of the swash plate.

Figure 5 analyzes the hydraulic moment of a single plunger on the swash plate, while the combined hydraulic moment of all plungers in one cycle is M_p . This paper specifies that a positive hydraulic moment causes an increase in the swash plate inclination, while a negative hydraulic moment causes a decrease.

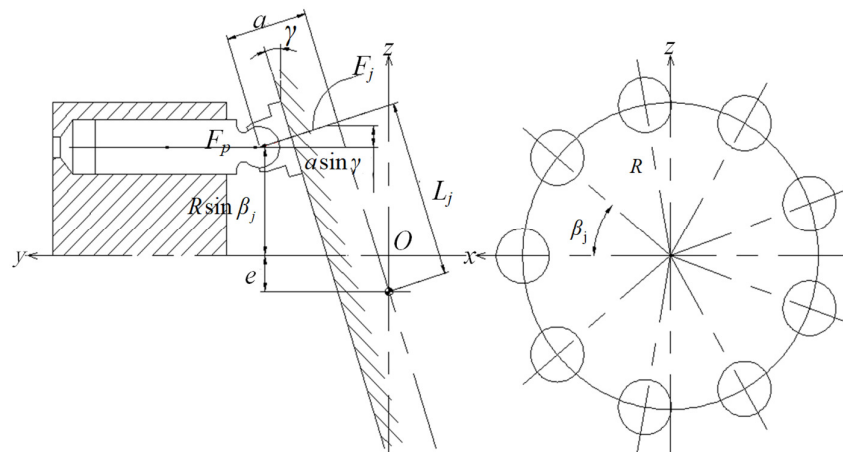


Figure 5. Hydraulic torque analysis of a single plunger on a swash plate.

Based on the dynamic analysis presented in Figure 5, it can be inferred that:

$$\begin{cases} F_j = \frac{F_p}{\cos \gamma} = \frac{P_j A}{\cos \gamma} \\ L_j = \frac{R \sin \beta_j + a \sin \gamma + e}{\cos \gamma} \end{cases} \quad (14)$$

where F_j is the hydraulic pressure of the j -th plunger on the swash plate, N, $j \in [1, Z]$; F_p is the hydraulic pressure on the plunger, N; P_j is the hydraulic pressure in the j -th plunger chamber, Pa; A is the area of the plunger, m^2 ; L_j is the length of the arm from F_j to the swash plate rotating shaft, m; R is the radius of the plunger distribution circle, m; β_j is the circumference distribution position of the j -th plunger, $\beta_j = \beta + \beta_1 + 2(j - 1)\pi/Z$, rad; β is the cylinder block angle, rad; $\beta = \omega t$, $\omega = 2\pi n/60$, ω is the rotation angular speed of the cylinder block, rad/s; a is the offset distance between the force point of the plunger ball head and the rotating shaft of the swash plate, m; and e is the eccentricity of the swash plate, m.

This paper stipulates that a is positive when the swash plate rotor axis is located to the right of the force point of the plunger ball head, and negative when the opposite is true; e is positive when the rotor axis is moving in the direction of the upper dead center of the plunger movement (the plunger is fully extended), and negative when the opposite is true. The combined hydraulic torque of each plunger on the swash plate is:

$$M_p = - \sum_{j=1}^Z F_j L_j = - \sum_{j=1}^Z \frac{P_j A (R \sin \beta_j + a \sin \gamma + e)}{\cos^2 \gamma} \quad (15)$$

During one cylinder block rotation cycle, the valve plate's structure affects the variation in the oil pressure, P_j , of each plunger chamber. This paper focuses on the asymmetric valve plate with a triangular vibration damping groove, whose structure and the corresponding plunger chamber pressure are shown in Figure 6.

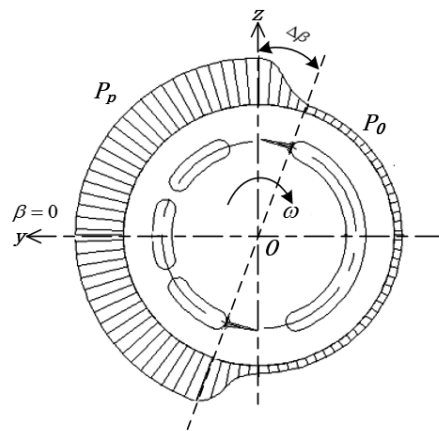


Figure 6. Structure of valve plate and pressure change in plunger chamber.

When the pump cylinder rotates one revolution, each plunger will pass through a high-pressure zone, a low-pressure zone, and two transition zones formed by the triangular damping groove.

In the transition zone, the pressure in the plunger chamber undergoes a nonlinear change, and its specific derivation process is more complicated. Usually, the effective method is to linearly approximate the plunger chamber pressure in the transition zone. This allows for obtaining a formula for the change in the plunger chamber pressure during the rotation period.

$$P_j = \begin{cases} P_p & \left(0 < \beta_j \leq \frac{\pi}{2} \right) \\ P_p - \frac{P_p - P_0}{\Delta\beta} \left(\beta_j - \frac{\pi}{2} \right) & \left(\frac{\pi}{2} < \beta_j \leq \frac{\pi}{2} + \Delta\beta \right) \\ P_0 & \left(\frac{\pi}{2} + \Delta\beta < \beta_j \leq \frac{3\pi}{2} \right) \\ P_0 + \frac{P_p - P_0}{\Delta\beta} \left(\beta_j - \frac{3\pi}{2} \right) & \left(\frac{3\pi}{2} < \beta_j \leq \frac{3\pi}{2} + \Delta\beta \right) \\ P_p & \left(\frac{3\pi}{2} + \Delta\beta < \beta_j \leq 2\pi \right) \end{cases} \quad (16)$$

where $\Delta\beta$ is the central angle corresponding to the pump triangular vibration damping groove, rad.

2.4.2. Inertia Torque of the Plunger on the Swash Plate

When the cylinder block rotates, the plunger moves in a reciprocating straight line relative to the block and rotates around the main shaft. The movement trajectory of the plunger ball head on the swash plate is an ellipse, as shown in Figure 7. When the plunger rotates at an angle of β around the central shaft from the top dead center position A to position B , the plunger ball head moves along an elliptical arc, AB . The projection of this

arc on the surface, Oxy , is an arc, AB' . Based on the geometric relationship, the axial displacement of the plunger can be determined as follows:

$$S = R \tan \gamma (1 - \cos \beta) \tag{17}$$

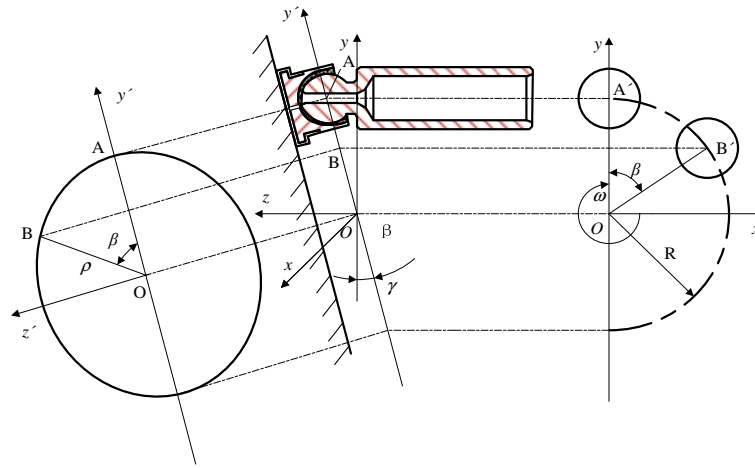


Figure 7. Movement path of the plunger ball head.

During the process of changing the swash plate inclination and cylinder block rotation, the speed and acceleration of the j -th plunger's axial motion are:

$$\begin{cases} v_j = \dot{S} = R [\dot{\gamma} \sec^2 \gamma (1 - \cos \beta_j) + \omega \tan \gamma \sin \beta_j] \\ a_j = \ddot{S} = R [\ddot{\gamma} \sec^2 \gamma (1 - \cos \beta_j) + 2\dot{\gamma}^2 \tan \gamma \sec^2 \gamma (1 - \cos \beta_j) + 2\omega \dot{\gamma} \sec^2 \gamma \sin \beta_j + \omega^2 \tan \gamma \cos \beta_j] \end{cases} \tag{18}$$

where v_j represents the axial motion speed of the j -th plunger, m/s; a_j represents the axial motion acceleration of the j -th plunger, m/s².

Then, the combined inertia moment of each plunger on the swash plate is:

$$M_1 = \sum_{j=1}^Z \frac{m_p a_j}{\cos \gamma} L_j = \sum_{j=1}^Z \frac{m_p a_j (R \sin \beta_j + a \sin \gamma + e)}{\cos^2 \gamma} \tag{19}$$

Equation (19) shows that the combined inertia moment of each plunger to the swash plate changes periodically. However, since the mass of the plunger is usually small, the combined moment amplitude is also tiny.

2.4.3. Frictional Torque of Swash Plate Rotation

The swash plate is fixed to the piston pump housing by two bearings, and when the swash plate rotates, it is subjected to frictional resistance torque from the bearings. This torque is affected by the pressure of the pump inlet and discharge chambers. The average value of this resistance can be expressed as:

$$M_2 = \frac{\pi d^2 Z r_1 f_1}{8 \cos \gamma} (P_p + P_0) \tag{20}$$

where r_1 is the radius of the swash plate support axis, m; f_1 is the bearing friction coefficient at the swash plate support. Since r_1 and f_1 are usually small, the frictional torque M_2 value is small.

2.4.4. Frictional Torque between the Plunger Ball Head and the Boot Ball Groove

When the swash plate rotates, the plunger ball head and the shoe ball groove slide relative to each other, resulting in frictional torque. This torque is also affected by the pressure of the pump inlet and discharge chamber, and can be expressed as an average value:

$$M_3 = \frac{\pi d^2 Z r_2 f_2}{8 \cos \gamma} (P_p + P_0) \quad (21)$$

where r_2 is the radius of the plunger ball head, m; f_2 is the friction coefficient between the plunger ball head and the boot ball groove. Similar to M_2 , because r_2 and f_2 are usually small, the value of frictional torque M_3 is small.

2.4.5. Self-Weight Torque

When the swash plate's gravity center does not fall on the rotating axis of the swash plate, the gravity of the swash plate will produce a self-weight torque, the magnitude of which is:

$$M_4 = Gb \cos \gamma \quad (22)$$

where G is the weight of the swash plate, N; b is the distance between the swash plate's gravity center and the rotating axis, m. Because b is usually tiny, the self-weight torque, M_4 , of the swash plate is small.

2.5. Piston Pump Output Characteristic Model

The pump outlet flow continuity equation is as follows:

$$Q_p = k_Q \gamma - C_p P_p - \frac{V_p}{\beta_e} \dot{P}_p \quad (23)$$

where Q_p is the load flow rate of the pump, m^3/s ; k_Q is the flow coefficient, $k_Q = n\pi d^2 D_p Z/4$, m^3/s ; n is the spindle speed, r/min ; d is the diameter of the plunger, m; D_p is the diameter of the plunger distribution circle, m; Z is the number of plungers; C_p is the leakage coefficient in the pump, $\text{m}^3/(\text{Pa}\cdot\text{s})$; P_p is pump outlet pressure, Pa; and V_p is the pump outlet volume, m^3 .

Rewrite Equation (23) as:

$$\dot{P}_p = \frac{\beta_e}{V_p} k_Q \gamma - \frac{\beta_e C_p}{V_p} P_p - \frac{\beta_e}{V_p} Q_p \quad (24)$$

By taking state variables $[x_1, x_2, x_3, x_4]^T = [\gamma, \dot{\gamma}, P_L, P_p]^T$ and combining Equations (5), (12), (13) and (24), the state space equation of the SAIP system can be obtained as follows:

$$\begin{cases} \dot{x}_1 = x_2 \\ \dot{x}_2 = C_1 x_1 + C_2 x_2 + C_3 x_3 + \varphi(x) \\ \dot{x}_3 = g(x, u)u + C_5 x_2 + C_4 x_3 \\ \dot{x}_4 = C_6 x_1 + C_7 x_4 + C_8 Q_p \end{cases} \quad (25)$$

where $C_1 = -\frac{K}{m}$, $C_2 = -\frac{B_p}{m}$, $C_3 = -\frac{A_p}{mL}$, $C_4 = -\frac{C_L \beta_e}{V}$, $C_5 = \frac{A_p L \beta_e}{V}$, $C_6 = \frac{k_Q \beta_e}{V_p}$, $C_7 = -C_p \beta_e / V_p$, $C_8 = -\beta_e / V_p$, $\varphi(x) = \frac{M(x)}{mL^2} + \frac{K}{m} (\frac{x_0}{L} + \gamma_{max})$, $M(x)$ is the other torque M , subjected to the swash plate mentioned above, $g(x, u) = \frac{\beta_e}{V} k_c [S(u) \sqrt{P_p - P_L} + S(-u) \sqrt{P_L - P_0}]$. To facilitate writing in the derivation process, $\varphi(x)$ and $M(x)$ are abbreviated as φ and M , respectively, in the rest of the paper.

Since the modulus of elasticity of the oil, pump leakage coefficient, etc., are affected by factors such as air content and temperature in the fluid, which are time-varying parameters, and then combined with Equation (25), it can be seen that the SAIP system is a fourth-order nonlinear time-varying system.

3. Simulation Study of SAIP's Output Characteristics

In this section, the SAIP simulation model is developed in Simulink, and the output characteristics and the influencing factors are explored in the simulation. The output characteristics of the SAIP refer to the dynamic characteristics of the pump outlet pressure and output flow rate.

In the simulation model, the load is simulated with a throttled hole, and the magnitude of the load is changed by changing the diameter of the hole, and its flow–pressure equation is:

$$Q_p = C_d \frac{\pi d_f^2}{4} \sqrt{\frac{2(P_p - P_0)}{\rho}} \quad (26)$$

where C_d is the throttling coefficient; d_f is the hole's diameter, m.

The SAIP model established in Simulink consists of four parts: the electro-hydraulic servo valve input voltage part, the load part, the servo pump body part, and the servo pump status display part. When the control voltage is positive, the high-pressure fluid enters the control piston cavity through the servo valve, so that the control piston rod pushes the swash plate inclination to reduce; when it is negative, the high-pressure fluid in the control piston cavity returns to the oil tank through the servo valve, and the swash plate inclination increases under the action of other swash plate moments (mainly for the combination of hydraulic torque and offset spring torque), and pushes the control piston rod to retract at the same time. The parameters used in the simulation are shown in Table 1. The solver set in Simulink is the Bogacki–Shampine solver, which computes the state of the model as an explicit function of the current value of the state and the state derivatives, which belongs to the fixed-step solver. The step size is set to 0.0001 s.

Table 1. Simulation parameters of the SAIP.

Parameter	Value	Unit	Parameter	Value	Unit
n	2000	r/min	V_p	6.28×10^{-7}	m^3
D	4.66×10^{-2}	m	I_s	5.76×10^{-4}	$\text{kg} \cdot \text{m}^2$
e	-1.2×10^{-3}	m	β_e	1.5×10^9	Pa
d	1.21×10^{-2}	m	ρ	840	kg/m^3
L	4.53×10^{-2}	m	P_0	0	Pa
x_0	1.16×10^{-2}	m	k_Q	1.6×10^{-3}	m^3/s
m_p	9.9×10^{-3}	kg	γ_{max}	$23\pi/360$	rad
B_p	0.6521	N·s/m	k_c	7.27×10^{-10}	$\text{m}^3/(\text{s} \cdot \text{V} \cdot \text{Pa}^{1/2})$
C_L	1.60×10^{-13}	$\text{m}^3/(\text{Pa} \cdot \text{s})$	C_d	0.7	1
V_0	2.83×10^{-7}	m^3	$\Delta\beta$	0.074	rad
K	1.78×10^{-4}	N/m	d_p	1.2×10^{-2}	m
C_p	1.60×10^{-13}	$\text{m}^3/(\text{Pa} \cdot \text{s})$	d_f	2×10^{-3}	m

3.1. Effect of Offset Spring's Stiffness on Output Characteristics

The function of the offset spring is to control the swash plate at maximum inclination in the initial state of the pump, allowing for maximum flow output. Additionally, it provides part of the return torque during the swash plate rotation process. If the offset spring's stiffness is too tiny, the swash plate may return weakly or even jam, resulting in no flow output from the pump and potentially causing severe accidents. Conversely, if the stiffness is too great, the swash plate may not be easily driven by the variable displacement mechanism, resulting in a slow displacement adjustment and reduced performance. Therefore, it is necessary to investigate the impact of the offset spring's stiffness on the SAIP's output characteristics.

The offset spring's stiffness of the SAIP mentioned above was 17.8 kN/m. For the sake of obvious comparison, the offset spring's stiffness values of the control group were taken to be 1.78 kN/m and 178 kN/m. The swash plate initial inclination was set to 0° , and the electro-hydraulic servo valve input voltage was -4 V (because the larger reverse

voltage makes the control piston chamber return oil smoothly: this excludes the effect of the servo valve on the swash plate dynamics and highlights the role of the offset spring). The dynamic characteristics of the swash plate and the output characteristics of the SAIP during the rotation of the swash plate to the maximum inclination angle were explored through a simulation, and the results are shown in Figures 8 and 9.

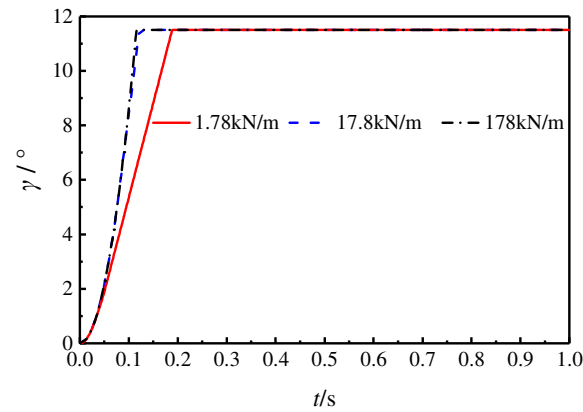


Figure 8. Swash plate inclination with different offset spring's stiffness.

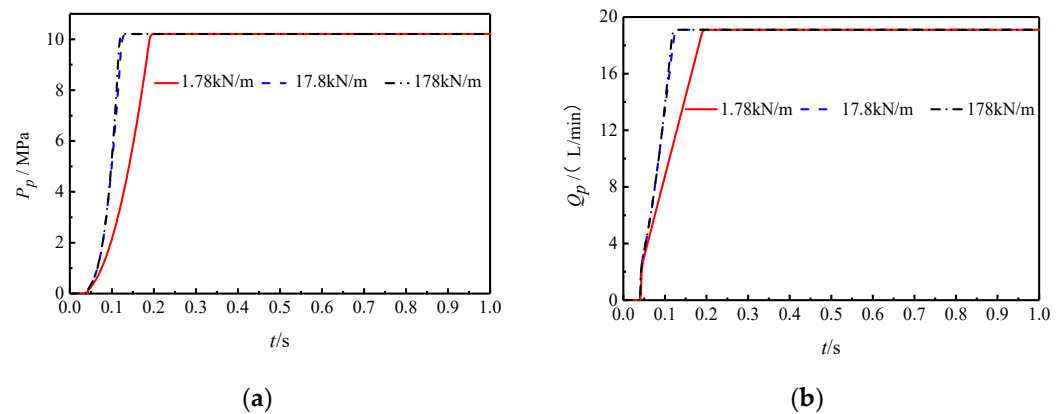


Figure 9. Output characteristics with different offset spring's stiffness. (a) Pump outlet pressure; (b) pump output flow.

Figure 8 indicates that increasing the offset spring's stiffness from 1.78 kN/m to 17.8 kN/m reduces the swash plate's return time from minimum to maximum inclination by half. However, there is no significant reduction in the return time when the stiffness is increased from 17.8 kN/m to 178 kN/m. Increasing the stiffness in the small stiffness stage improves the return speed. However, the effect is no longer significant after a certain point. Additionally, excessively high stiffness increases the volume, weight, and the load of the variable displacement mechanism, leading to a slow displacement adjustment. The conclusion drawn from the analysis can be used to determine the offset spring's stiffness for the piston pump design.

It can be seen from Figure 9 that the change rule of pressure and flow rates is basically the same as the change rule of swash plate inclination with different spring stiffness. The only notable difference is that the swash plate inclination increases in the first 0.05 s while the pressure and flow rates remain at 0. The reason is that the oil output from the pump needs to fill the pipe and flow out of the throttle orifice before the pressure can be established. This process takes a certain amount of time, resulting in zero pressure and flow rate for the first 0.05 s.

3.2. Effect of Control Piston's Diameter on Output Characteristics

The control piston's role is to push the swash plate to reduce its inclination. When the oil pressure in the control piston chamber is constant, the force of the control piston rod acting on the swash plate is determined by the control piston's cross-sectional area, so the control piston's diameter will affect the dynamics of the swash plate inclination, and then affect the output characteristics of the SAIP.

The study simulated the output characteristics of a SAIP with a control piston diameter of 12 mm and compared it to control groups with control piston diameters of 6 mm, 8 mm, and 16 mm. The initial inclination was set to 11.5° , and the servo valve input voltage was 1 V. The output characteristics in reducing the swash plate inclination driven by the control piston rod were explored. The results are presented in Figures 10 and 11.

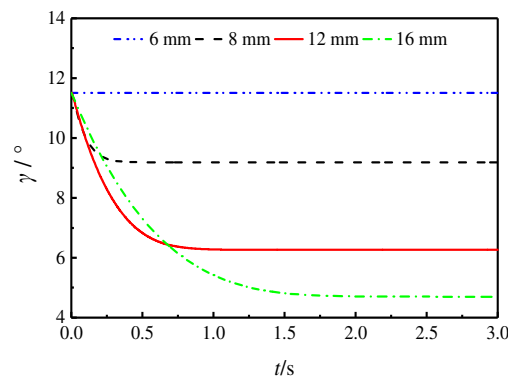


Figure 10. Swash plate inclination with different control piston diameters.

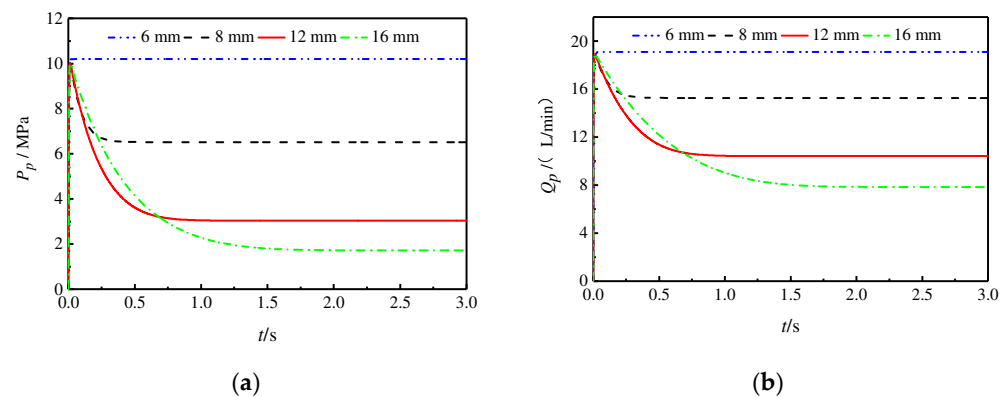


Figure 11. Output characteristics with different control piston diameters. (a) Pump outlet pressure; (b) pump output flow.

Figure 10 demonstrates that when the control piston's diameter is 6 mm, the control piston rod cannot push the swash plate. As the diameter increases to 8 mm and 12 mm, the speed of swash plate inclination reduction also increases. However, when the control piston's diameter is 16 mm, the speed of the swash plate inclination reduction is lower than that of 8 mm and 12 mm. This is because, when the piston diameter is increased, the chamber volume also increases, requiring more oil to enter. The opening of the servo valve restricts the speed of oil entering, resulting in a lower rate of swash plate inclination when the control piston's diameter is 16 mm. It is evident that the variable displacement mechanism cannot push the swash plate when the diameter is too small. Increasing the diameter can improve the variable displacement mechanism's action speed, but it can reduce the speed if it is too large. This conclusion can guide the determination of the control piston's diameter in the SAIP design.

It should be pointed out that the SAIP studied in this paper is a self-supplied pump. That is, the oil source of the servo valve is the pump outlet oil. When the load is constant, the

swash plate inclination decreases, causing the pump displacement and outlet oil pressure to decrease. Eventually, the variable displacement mechanism will not push the swash plate, and it will stabilize at a certain angle. This is a significant characteristic of the self-supplied servo pump. Therefore, in Figure 10, the swash plate is stabilized at a certain angle. The larger the control piston's diameter, the greater the force of the control piston rod on the swash plate. As a result, the swash plate is stabilized at a smaller angle.

The analysis of Figure 11 shows that the change rule of pressure and flow rates is basically the same as the change rule of inclination with different control piston diameters. However, since the SAIP is self-supplied, there is no high-pressure oil in the control piston chamber before starting, and the displacement adjustment begins almost until the pump has wholly established the pressure. Figure 11 shows that the process of increasing pressure takes about 0.02 s.

3.3. Effect of Rotation Speed on Output Characteristics

To study the effect of rotation speed on the output characteristics of the SAIP, the servo valve voltage is taken to be 0 V, and the rotational speeds are taken to be 800 r/min, 1200 r/min, 1600 r/min, and 2000 r/min for the simulation. The other parameters are shown in Table 1, and the simulation results are shown in Figure 12.

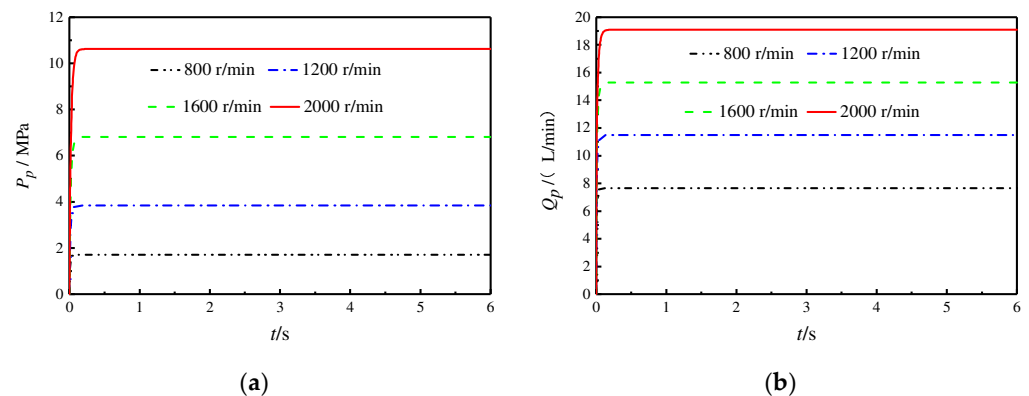


Figure 12. Output characteristics with different rotation speeds. (a) Pump outlet pressure; (b) pump output flow.

Figure 12 shows that the higher the rotation speed, the higher the output flow and the higher the pressure formed. However, the flow rate and speed are not strictly proportional. As can be seen from the figure, the steady-state flow rate is 7.8 L/min at 800 r/min and 19 L/min at 2000 r/min. The magnitude of the flow rate increase did not change to 2.5 times the initial magnitude as well as the rotational speed. The main reason is that the system pressure increases, and the leakage in the pump increases, resulting in a lower output flow. The results show that the pump's flow rate is not strictly proportional to the displacement, and the higher the load, the smaller the pump's output flow at the same speed.

In order to visually show the influence of rotational speed on the flow rate and pressure, the steady-state average values of the flow rate and pressure at different speeds were calculated, and the fitting curves of the flow rate and pressure with speed were drawn according to the results, as shown in Figure 13.

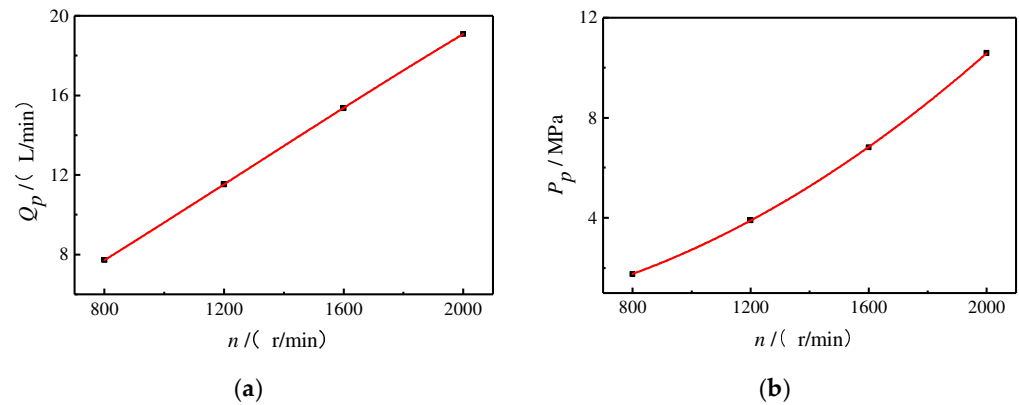


Figure 13. (a) Fitting curve of flow rate variation with speed; (b) fitting curve of pressure variation with speed.

As can be seen in Figure 13a, the flow rate is almost proportional to the speed, and it can be seen in Figure 13b that under the condition of a certain load, the pressure at the outlet of the servo pump has an obvious nonlinear relationship with the speed, and the relationship curve is convex. With the increase in the rotational speed, the rate of change in pressure also increases gradually, that is, under the same rotational speed increase, the higher the rotational speed, the greater the increase in pressure. This law is also consistent with the pressure–flow equation of the throttling holes.

3.4. Effect of Servo Valve's Input Voltage on Output Characteristics

To investigate the effect of the servo valve's input voltage on the output characteristics of the SAIP, this section simulates the two processes of decreasing and increasing the swash plate inclination.

3.4.1. The Process of Decreasing the Swash Plate Inclination

The servo valve's input voltages were taken as 0.15 V, 0.3 V, and 0.5 V, the initial swash plate inclination was set to 11.5° , other parameters are shown in Table 1, and the simulation results are shown in Figure 14.

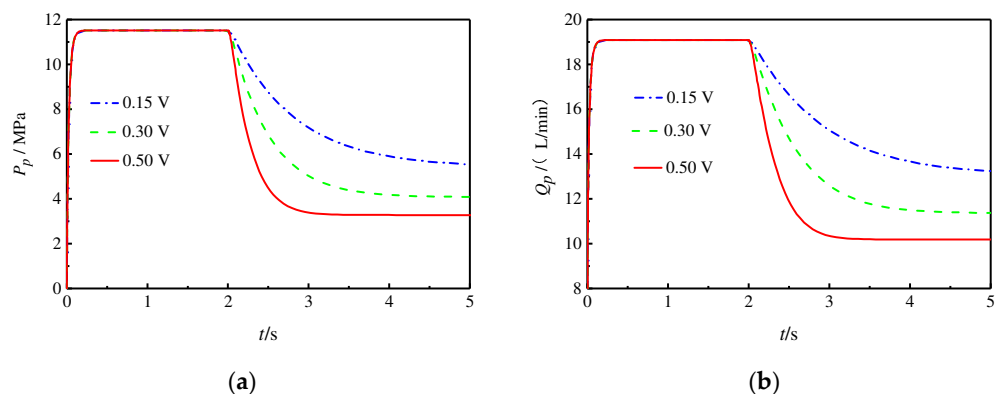


Figure 14. Output characteristics with different servo valve input voltages. (a) Pump outlet pressure; (b) pump output flow.

Figure 14 shows that as the voltage increases, the change in displacement accelerates significantly. However, because of the self-supplied characteristics, as seen in the previous section, the swash plate inclination will be stabilized at a specific value, so the pump outlet pressure and output flow rate will also be stabilized to a particular value. At a steady state, although oil is still flowing into the control piston chamber, while the control piston chamber has leakages, the inflow of oil just compensates for the oil leakage, so the control

piston no longer moves. The voltage increases, the servo valve opening increases, the throttling effect on the oil decreases, and the final oil pressure of the control piston chamber can be higher, which can make the swash plate stable at a smaller angle, so the pump outlet pressure and output flow can also be stable at a smaller value.

3.4.2. The Process of Increasing the Swash Plate Inclination

The servo valve voltage was set to 0 V for the first 0.6 s, 4 V for 0.6~1 s, and -0.15 V, -0.3 V, and -0.5 V after 1 s. The purpose of this setting is to wait for the SAIP to establish the outlet pressure fully, then adjust the swash plate to the smallest angle that can be achieved, and then let the swash plate return to the position to explore the pressure and flow dynamics of the SAIP with different reverse voltages. The results are shown in Figure 15.

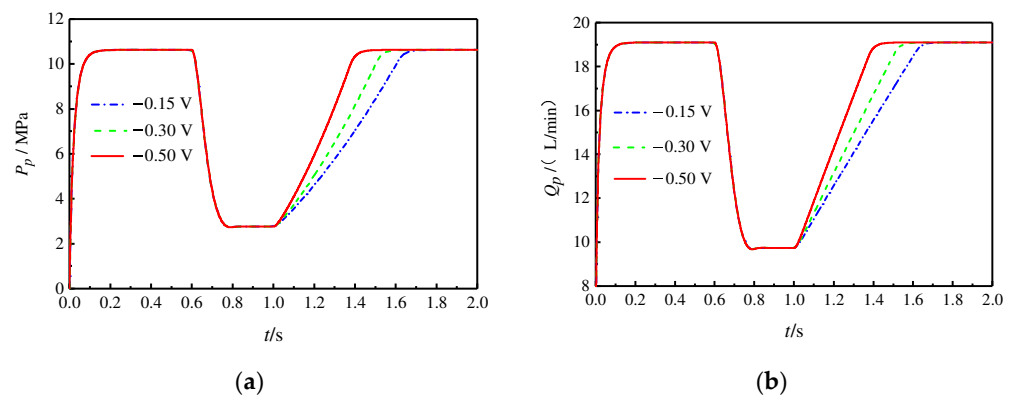


Figure 15. Output characteristics with different servo valve input voltages (negative voltages). (a) Pump outlet pressure; (b) pump output flow.

Figure 15 shows that as the voltage increases in the reverse direction, the outlet pressure and output flow rate to return to the maximum time value continue to shorten. The reason is that the voltage increases, the servo valve opening increases, the throttling effect of the oil in the control piston chamber is weakened, the oil is more accessible to return to the tank, and the swash plate is more straightforward to return to the position. A comparison with the simulation results of controlling the swash plate inclination to decrease shows that for the same voltage, the time required for the swash plate to return to the maximum value is shorter, about half the time needed for the former.

4. Experimental Validation

4.1. Experimental Bench

The experimental platform built for the SAIP, as shown in Figure 16, mainly consists of two major systems: one is the mechanical–hydraulic system, mainly including an oil tank, drive motors, cooling fans, throttle valves, relief valves, a variety of switching valves, as well as flow and pressure sensors; and the other is the measurement and control system, which mainly consists of the power cabinets, signal cabinets (including Siemens S7-1200 PLC), a junction box, and human–computer interaction equipment. Table 2 shows the information on the main sensors.

Table 2. Main sensors of the experimental platform.

Sensors	Signals	Range	Precision
Pressure sensor	0–10 V	0–30 MPa	$\pm 0.2\%$ FS
Flow rate sensor	4–20 mA	1–40 L/min	$\pm 0.2\%$ FS
Rotational speed sensor	5–15 kHz	0–8000 rpm	$\pm 0.2\%$ FS

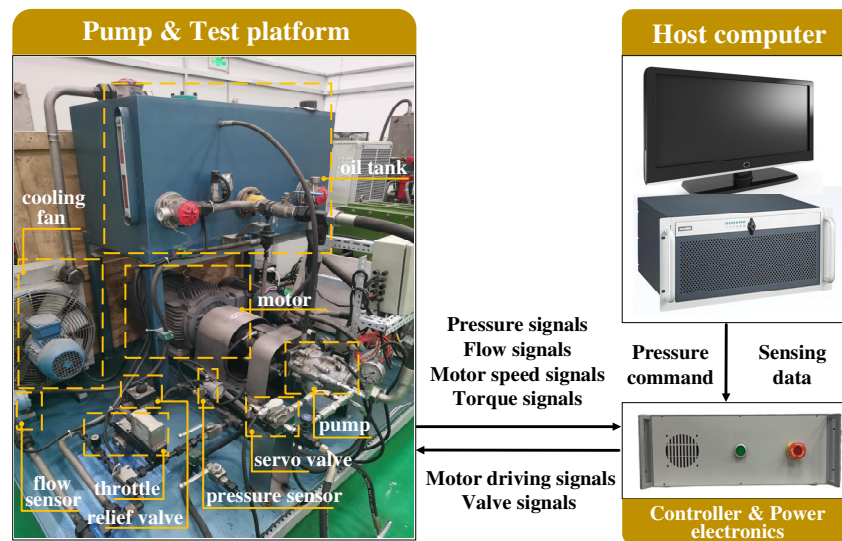


Figure 16. Experimental platform.

The working principle of the experimental system is that the industrial computer communicates with the PLC through the Ethernet line as the host computer, and the PLC collects the signals from each sensor as the lower computer. After receiving instructions from the host computer, the PLC outputs the control signal to the electro-hydraulic servo valve according to the written control program. Then, the electro-hydraulic servo valve adjusts the swash plate inclination by controlling the high-pressure oil in and out of the control piston chamber and realizes the accurate control of the output flow rate and outlet pressure of the SAIP through variable displacement.

The intelligent pump prototype is transformed from an aviation constant-pressure variable displacement pump, which can be realized by replacing the valve core of the pressure regulator and connecting the servo valve pipeline outside the pump. Table 3 shows the parameters of the intelligent pump prototype.

Table 3. Parameters of the SAIP prototype.

Parameters	Values
Rated pressure p_{rated} (MPa)	21
Rated displacement V_p (mL/r)	9.5
Maximum rotation speed n (rpm)	4200
The rated flow rate of the servo valve Q_{sv} (L/min)	2
Rated current of the servo valve I_{sv} (mA)	± 10

It is worth noting that the signals collected by the sensors will be affected by their measurement accuracy, leading to certain errors. At the same time, electromagnetic noise will also affect the signal when transmitting to the controller, resulting in a certain oscillation. The combination of these factors can lead to uncertainty in signal measurements. This uncertainty can be reduced to an acceptable range by selecting a high-precision sensor and employing a suitable filtering algorithm.

4.2. Experiments on the Output Characteristics of the SAIP

The experiment used two working conditions to explore the effects of different rotation speeds and servo valve input voltages on the output characteristics. The opening of the throttle valve was kept constant to maintain a constant load.

4.2.1. Experimental Results

(1) Effect of Rotation Speed on Output Characteristics

The servo valve voltage was set to 0 V. The experiments were carried out by using the rotational speeds of 800 r/min, 1200 r/min, 1600 r/min, and 2000 r/min, and the experimental results are shown in Figure 17.

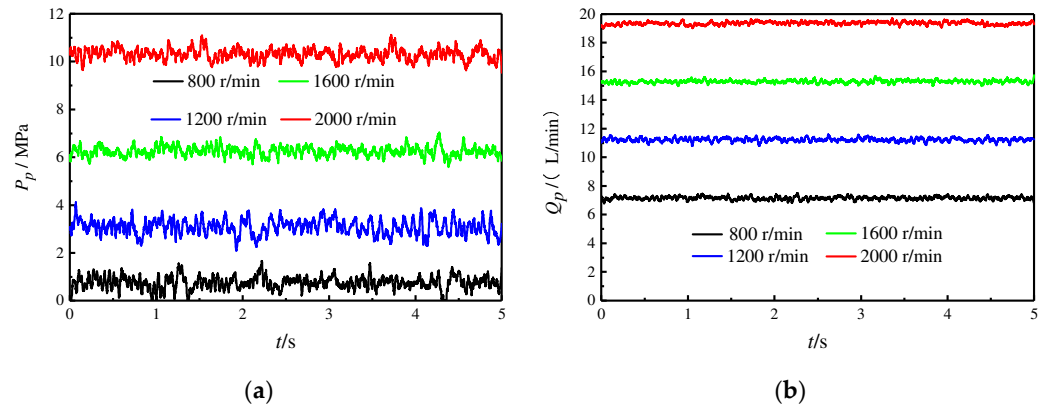


Figure 17. Output characteristics with different rotation speeds (experimental results). (a) Pump outlet pressure; (b) pump output flow.

Figure 17 demonstrates that as the rotational speed increases, the servo pump's flow rate and outlet pressure also increase. And it can be found that when the speed increases by the same amount, the increase in flow rate is almost the same, but the increase in pressure is becomes larger and larger, that is, with the increase in speed, the law of change in pressure becomes larger and larger. It can be seen that the relationship between the flow rate and rotational speed is almost linear, and the relationship between the pressure and rotational speed should be nonlinear. This law can be further understood by the pressure–flow equation of the throttling holes. The flow rate is proportional to the square root of the pressure, so the pressure increases exponentially as the flow rate increases almost linearly with the rotational speed.

In addition, compared to the simulation results, it can be observed that the flow and pressure curves at a steady state show more obvious oscillations. In addition to the measurement noise to which the sensor signal is subjected, axial piston pumps' inherent flow and pressure pulsation characteristics are the main cause of this oscillation. The instantaneous flow rate of a single plunger can be deduced from the principle of axial piston pump as

$$q' = \frac{\pi d^2 D}{4} \omega \tan \gamma \sin \omega t \quad (27)$$

It can be seen that the instantaneous flow rate of a single plunger varies according to a sinusoidal law. The instantaneous flow rate of the whole pump is the sum of the instantaneous flow rates of several plungers in the oil compression zone, so it is also pulsating. The self-supplied aviation intelligent pump model established in this paper focuses on the output characteristics of this novel scheme, thus simplifying the modeling of the flow pulsation characteristics common to axial piston pumps.

The average flow rate and pressure values were calculated at different rotational speeds to visualize the relationship between the flow rate, pressure, and rotational speed. Then, the fitted curves of the flow rate and pressure with rotational speed were plotted based on the data in Table 4, as shown in Figure 18.

Table 4. Average flow rate and pressure of the SAIP at different speeds.

Rotate Speed (r/min)	Flow Rate (L/min)	Pressure (MPa)
800	7.15	0.75
1200	11.23	3.09
1600	15.29	6.26
2000	19.37	10.32

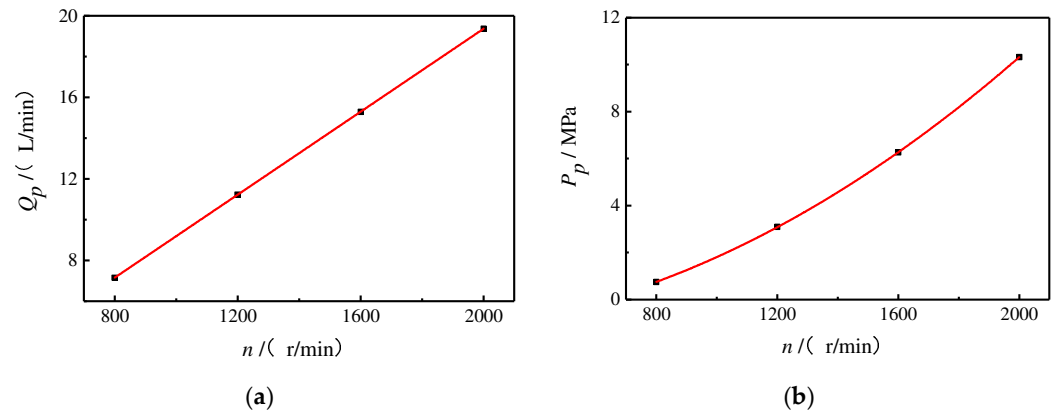


Figure 18. (a) Fitting curve of flow rate variation with speed; (b) fitting curve of pressure variation with speed (experimental results).

Figure 18a shows that the flow rate is nearly proportional to the rotation speed. However, upon closer examination, the theoretical flow rate at 800 r/min should be 7.75 L/min compared to 2000 r/min, while the actual flow rate is 0.6 L/min less. This is due to the low speed at 800 r/min, which results in insufficient oil suction, causing the actual output flow rate to be less than the theoretical flow rate. It is evident that the rotation speed of the SAIP must not be too low during operation, as this may result in inadequate oil suction. This also indicates that the use of adjustable rotation speed to control the output flow rate will be limited by the minimum flow rate due to the minimum speed. When the rotational speed is lower than the limit, it will cause the piston pump to have insufficient oil suction, causing suction cavitation and reducing the life of the piston pump. It can be seen that the electro-hydraulic servo variable displacement method adopted by the SAIP does not have this problem and has more advantages.

Figure 18b indicates that the outlet pressure has a clear nonlinear relationship with the speed at a specific load, and the relationship curve is convex, which is also in line with the pressure–flow equation of the throttle orifice.

(2) Effect of Servo Valve’s Input Voltage on Output Characteristics

Set the rotation speed to 2000 r/min, and at the 2nd s, set the servo valve’s input voltage to 0.15 V, 0.3 V, and 0.5 V, for the experiment, and the results are shown in Figure 19 and Table 5.

Table 5. Steady-state flow rate, average pressure, and setting time of servo pump under different voltage tests.

Voltage (V)	Flow Rate (L/min)	Pressure (MPa)	Setting Time (s)
0.15	14.45	6.03	1
0.3	12.20	4.04	0.5
0.5	11.59	3.56	0.3

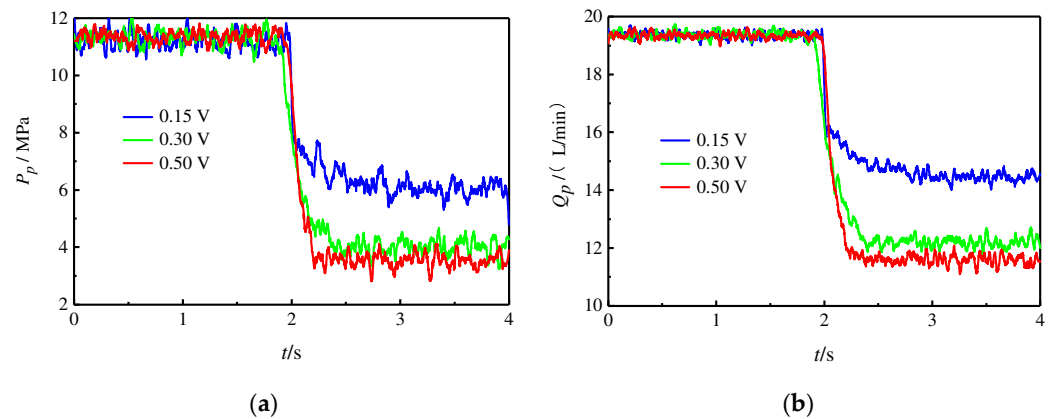


Figure 19. Output characteristics with different servo valve input voltages (experimental results). (a) Pump outlet pressure; (b) pump output flow.

It can be seen that as the voltage increases, the adjustment time of the SAIP is significantly reduced. The outlet pressure and output flow have a lower limit, and the lower limit decreases with an increasing voltage. The reason is that the oil source of the servo valve is the pump outlet oil. The servo valve oil supply pressure is also reduced when the pump outlet pressure drops. When reduced to a specific value, the control piston rod can no longer push the swash plate. Therefore, there is a lower limit to the SAIP's flow rate and pressure. After entering the steady state, although the oil continues to flow into the control piston cavity, there is an internal leakage in the control piston cavity, resulting in the inflow of oil just to compensate for the leaked oil, so the control piston no longer moves. The analysis shows that the larger the servo valve voltage, the smaller the throttling effect on the oil, so the oil pressure in the control piston cavity is higher, and the control piston rod can push the swash plate to stabilize at a smaller angle. Hence, the lower limit of the SAIP's outlet pressure and output flow rate is lower.

4.2.2. Comparison of Simulation and Experimental Results

To verify the accuracy of the SAIP model established in this paper, the experimental results are compared with the simulation results, as shown in Figures 20–23.

Figures 20 and 21 show that the experimental results at different rotation speeds and simulation results in the trend are basically the same, only in the numerical value of the slight difference. The subtle differences are mainly due to the fact that the simulation parameters are not precisely the same as the actual physical system's parameters, and there are flow pulsations, pressure pulsations, external disturbances, and sensor noise in the actual system, which are not easy to be considered in simulation conditions.

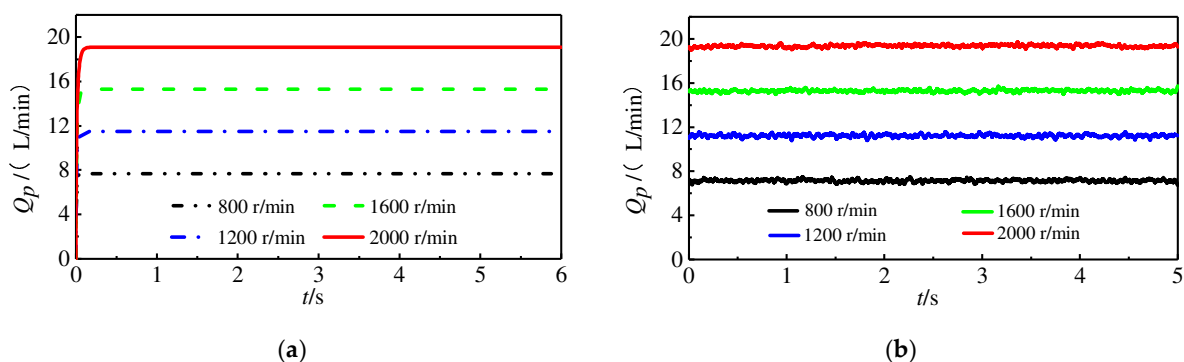


Figure 20. Simulation and experimental results comparison of output flow at different speeds. (a) Simulation results; (b) experimental results.

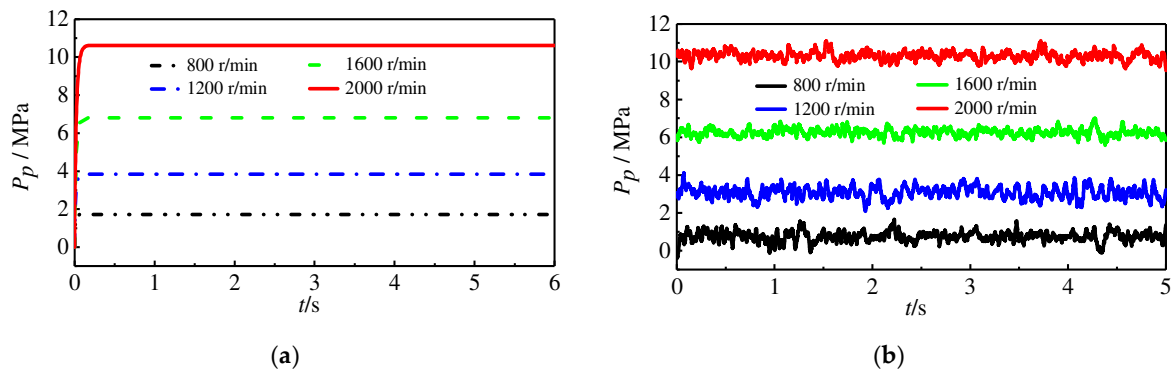


Figure 21. Simulation and experimental results comparison of outlet pressure at different speeds. (a) Simulation results; (b) experimental results.

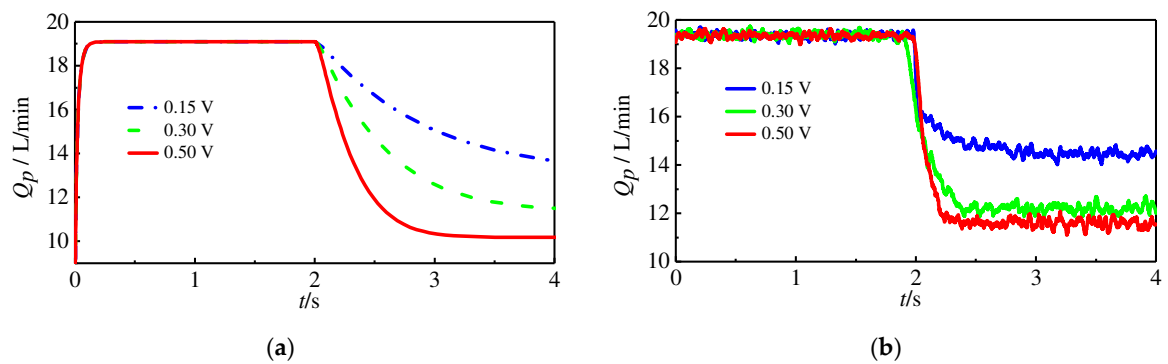


Figure 22. Simulation and experimental results comparison of output flow at different voltages. (a) Simulation results; (b) experimental results.

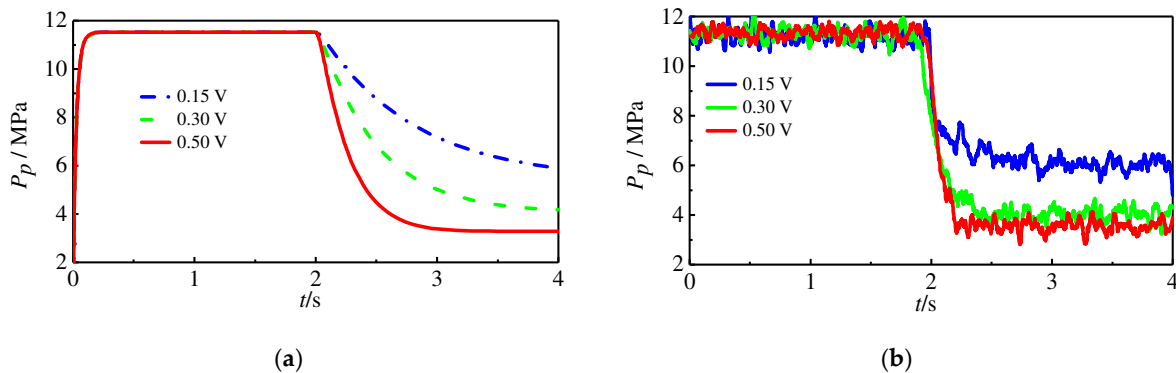


Figure 23. Simulation and experimental results comparison of outlet pressure at different voltages. (a) Simulation results; (b) experimental results.

As can be seen in Figures 22 and 23, both the simulation and experimental results show that as the servo valve's input voltage increases, the displacement change accelerates. There are lower limits for the flow and pressure; the larger the voltage, the lower the limit. Under different servo valve input voltages, the simulation results are consistent with the experimental results regarding the change trend.

From the above comparison results, it can be seen that the model established in this paper can genuinely reflect the physical laws of the SAIP, which is correct and credible. Based on the model, the study of the vital structural parameters' effect on the output characteristics is also credible and can guide the design of critical structural parameters.

5. Conclusions

In this paper, a novel self-supplied aviation intelligent pump scheme is introduced. Based on the established nonlinear model, the influences of various structural parameters, such as the offset spring's stiffness and control piston's diameter, on the output characteristics of the SAIP are analyzed in detail, and the performance under different working conditions is investigated through experiments. The main conclusions are summarized as follows:

- (1) The scheme of a new SAIP is presented, which creatively draws oil from the pump outlet as the oil source of the servo valve that regulates the swash plate inclination. It has the advantages of a high power-to-weight ratio and a compact structure. It can be easily modified based on a widely used aviation constant-pressure variable displacement pump.
- (2) Based on the principal analysis of the system, especially the load torque of the swash plate, which is the key component to realize the variable displacement, it is analyzed in detail, and the output characteristic model of the system, including a variety of nonlinear characteristics, is established.
- (3) Based on the system dynamic model, several vital structural parameters, such as the offset spring's stiffness and the control piston's diameter, are simulated to study their influence on the output characteristics and to guide the design of the key structural parameters of the intelligent pump to meet the rapidity and effectiveness of the displacement adjustment.
- (4) The principal prototype and test bench of the SAIP are established, and the influence of rotational speed and servo valve's input voltage on the output characteristics are experimentally investigated. By comparing the results with the simulation, the established system model's accuracy is verified, laying the foundation for the design of the servo control strategy for the outlet pressure and flow of the SAIP.
- (5) The SAIP model established in this paper focuses on the output characteristics of this novel scheme, thus simplifying the modeling of the flow pulsation characteristics common to axial piston pumps. The follow-up research can take into account the characteristics of flow pulsation and pressure pulsation, and further improve the accuracy of the model of SAIP, so as to help the development of aviation intelligent hydraulic system.

Author Contributions: Conceptualization, Y.W. and X.H.; Methodology, X.H. and F.Y.; Resources, L.Y.; Validation, F.Y. and X.H.; Data curation, F.Y.; Writing—original draft preparation, X.H.; Writing—review and editing, Y.F. and L.Y.; project administration, Y.F. All authors have read and agreed to the published version of the manuscript.

Funding: This research received no external funding.

Data Availability Statement: The data presented in this study are available on request from the corresponding author.

Conflicts of Interest: The authors declare no conflicts of interest.

References

1. Li, T.; Wang, H.; Zhao, Q.; Duan, B.; Wu, T. General Scheme Study for Civil Aircraft Hydraulic Power System. In Proceedings of the CSAA/IET International Conference on Aircraft Utility Systems (AUS 2022), Nanchang, China, 17–20 August 2022; pp. 88–92. [\[CrossRef\]](#)
2. Wang, S.; Tomovic, M.; Liu, H. *Commercial Aircraft Hydraulic Systems*; Shanghai Jiao Tong University Press Aerospace Series; Elsevier Inc.: Amsterdam, The Netherlands, 2015; pp. 1–263.
3. Guo, S.; Chen, J.; Lu, Y.; Wang, Y.; Dong, H. Hydraulic piston pump in civil aircraft: Current status, future directions and critical technologies. *Chin. J. Aeronaut.* **2020**, *33*, 16–30. [\[CrossRef\]](#)
4. Mileti, J.A.; Lawhead, P.M. Controlled pressure pumps for more efficient hydraulic systems. *SAE Tech. Pap.* **1986**. [\[CrossRef\]](#)
5. Chen, B. Research on Aircraft Intelligent Pump System. Ph.D. Dissertation, Beihang University, Beijing, China, 1998.
6. Ma, J. Research on Intelligent Pump and its Experiment System. Ph.D. Dissertation, Beihang University, Beijing, China, 2004.

7. Fu, Y.; Qi, H.; Lu, Y.; Guo, R.; Li, Z.; Xue, J.; Yang, Q. A novel electrical servo variable displacement hydraulic pump used for integrated actuator in MEA. In Proceedings of the 28th Congress of the International Council of the Aeronautical Sciences, ICAS, Brisbane, Australia, 23–28 September 2012; pp. 3907–3912.
8. Qi, H.; Liu, S.; Yang, R.; Yu, Y. Research on new intelligent pump control based on sliding mode variable structure control. In Proceedings of the 14th IEEE International Conference on Mechatronics and Automation, ICMA, Takamatsu, Japan, 6–9 August 2017; pp. 1239–1244.
9. Wu, X.; Chen, C.; Hong, C.; He, Y. Flow ripple analysis and structural parametric design of a piston pump. *J. Mech. Sci. Technol.* **2017**, *31*, 4245–4254. [[CrossRef](#)]
10. Fang, X.; Ouyang, X.; Yang, H. Investigation into the effects of the variable displacement mechanism on swash plate oscillation in high-speed piston pumps. *Appl. Sci.* **2018**, *8*, 658. [[CrossRef](#)]
11. Pan, Y.; Li, Y.; Liang, D. The influence of dynamic swash plate vibration on outlet flow ripple in constant power variable-displacement piston pump. *Proc. Inst. Mech. Eng. Part. C J. Mech. Eng. Sci.* **2019**, *233*, 4914–4933. [[CrossRef](#)]
12. Chen, L.; Ye, S.; Chang, Z.; Gou, X.; Sun, K. Simulation research on the revolution-pressure performance of an aeronautical hydraulic axial piston pump. In Proceedings of the 2016 IEEE/CSAA International Conference on Aircraft Utility Systems, AUS, Beijing, China, 8–14 October 2016; pp. 1247–1251.
13. Kumar, N.; Kumar, R.; Sarkar, B.K.; Maity, S. Performance Analysis of the Swashplate Axial Piston Pump with Hydraulic Fluid Temperatures. *J. Sci. Ind. Res.* **2021**, *80*, 943–948.
14. De, I.; Sarkar, S.; Chaudhuri, S.; Mondal, N.; Kumar, N. Effect of Dynamic Swiveling Torque and Eccentricity on the Design of Compensator Cylinders for a Variable Displacement Axial Piston Pump—Modelling & Simulation. *Jordan J. Mech. Ind. Eng.* **2023**, *17*, 255–268.
15. Kemmetmüller, W.; Fuchshumer, F.; Kugi, A. Nonlinear pressure control of self-supplied variable displacement axial piston pumps. *Control Eng. Pract.* **2010**, *18*, 84–93. [[CrossRef](#)]
16. Mu, X.; Wang, J.; Wang, S. An improvement on a method for nonlinear pressure control of self-supplied variable displacement axial piston pumps. In Proceedings of the IFAC Proceedings Volumes (IFAC-PapersOnline), Milano, Italy, 28 August–2 September 2011; Elsevier: Amsterdam, The Netherlands, 2011; pp. 7216–7220.
17. Guo, K.; Xu, Y.; Li, J. A Switched Controller Design for Supply Pressure Tracking of Variable Displacement Axial Piston Pumps. *IEEE Access* **2018**, *6*, 3932–3942. [[CrossRef](#)]
18. Huang, X.; Xu, B.; Huang, W.; Xu, H.; Lyu, F.; Su, Q. Active pressure ripple reduction of a self-supplied variable displacement pump with notch least mean square filter. *Micromachines* **2021**, *12*, 932. [[CrossRef](#)] [[PubMed](#)]

Disclaimer/Publisher’s Note: The statements, opinions and data contained in all publications are solely those of the individual author(s) and contributor(s) and not of MDPI and/or the editor(s). MDPI and/or the editor(s) disclaim responsibility for any injury to people or property resulting from any ideas, methods, instructions or products referred to in the content.